

Evolution of ground state and upper critical field in $R_{1-x}Gd_xNi_2B_2C$ ($R = Lu, Y$): Coexistence of superconductivity and spin-glass state

S. L. Bud'ko, V. G. Kogan, H. Hodovanets, S.

Ran, S. A. Moser, M. J. Lampe, and P. C. Canfield

Ames Laboratory, US DOE and Department of Physics and Astronomy,

Iowa State University, Ames, Iowa 50011

(Dated: September 10, 2010)

Abstract

We report effects of local magnetic moment, Gd^{3+} , doping ($x \lesssim 0.3$) on superconducting and magnetic properties of the closely related $Lu_{1-x}Gd_xNi_2B_2C$ and $Y_{1-x}Gd_xNi_2B_2C$ series. The superconducting transition temperature decreases and the heat capacity jump associated with it drops rapidly with Gd-doping; qualitative changes with doping are also observed in the temperature-dependent upper critical field behavior, and a region of coexistence of superconductivity and spin-glass state is delineated on the $x - T$ phase diagram. The evolution of superconducting properties can be understood within Abrikosov-Gor'kov theory of magnetic impurities in superconductors taking into account the paramagnetic effect on upper critical field with additional contributions particular for the family under study.

PACS numbers: 74.70.Dd, 74.25.Dw, 74.62.Bf, 75.50.Lk

I. INTRODUCTION

With discoveries of new superconducting materials, classical results on effects of non-magnetic and magnetic impurities in superconductors^{1,2} are being continuously tested and augmented. For example, the searches for impurity-induced states in superconductors³ and for superconducting quantum critical points⁴⁻⁶ are few such topics. Unfortunately, in some studies of superconductors with magnetic impurities the emphasis is frequently on just the superconducting properties whereas the state of magnetic subsystem is often neglected.

The rare earth-nickel borocarbides ($\text{RNi}_2\text{B}_2\text{C}$, $\text{R} = \text{rare earth}$) present a rare opportunity to study, within the same family, superconductivity, complex, local moment, magnetism, and their coexistence, as well as physics of strongly correlated, heavy fermion materials.⁷⁻¹⁰ In this work we concentrate on thermodynamic and magneto-transport properties of $\text{LuNi}_2\text{B}_2\text{C}$ and $\text{YNi}_2\text{B}_2\text{C}$ superconductors with the non-magnetic rare earths (Lu or Y) partially substituted by magnetic moment bearing gadolinium. Pure $\text{LuNi}_2\text{B}_2\text{C}$ and $\text{YNi}_2\text{B}_2\text{C}$ have a conveniently high superconducting transition temperatures, T_c , and are readily available as well characterized single crystals. The details of the superconducting pairing in these materials are still debated, with exotic scenarios being examined.¹¹⁻¹⁵ Since the Gd^{3+} ion has a spherically symmetric, half-filled $4f$ shell, and therefore virtually no crystal electric field effects associated with it, using gadolinium as a magnetic rare earth dopant may simplify the problem at hand. Although in resistivity and low field dc magnetic susceptibility the features associated with a magnetic subsystem, if located below T_c , are often obscured by strong superconducting signal, it was shown¹⁶⁻¹⁸ that in this situation heat capacity measurements can provide a valuable insight. So far there were several publications, mainly on polycrystalline samples, on physical properties of $\text{Y}_{1-x}\text{Gd}_x\text{Ni}_2\text{B}_2\text{C}$ ¹⁹⁻²⁵ and $\text{Lu}_{1-x}\text{Gd}_x\text{Ni}_2\text{B}_2\text{C}$ ^{18,21,26,27} solid solutions. It is noteworthy that although different studies generally agree on the rate of suppression of T_c (on the pure $\text{YNi}_2\text{B}_2\text{C}$ side) and change of the Néel temperature, T_N , (on the pure $\text{GdNi}_2\text{B}_2\text{C}$ side) with x , separation (absence of coexistence) of the superconducting and antiferromagnetic order in $\text{Y}_{1-x}\text{Gd}_x\text{Ni}_2\text{B}_2\text{C}$ near $x = 0.3$ was alluded to in Ref. 25, whereas a coexistence of antiferromagnetism and superconductivity at some region of intermediate concentrations was suggested in Refs. 20,23. Additionally, non-monotonic temperature dependence of the upper critical field, $H_{c2}(T)$, was reported for $\text{Lu}_{0.88}\text{Gd}_{0.12}\text{Ni}_2\text{B}_2\text{C}$.²⁷

A comparative study of the effects of Gd-doping on T_c , $H_{c2}(T)$ and the state of magnetic

sublattice in $\text{Lu}_{1-x}\text{Gd}_x\text{Ni}_2\text{B}_2\text{C}$ and $\text{Y}_{1-x}\text{Gd}_x\text{Ni}_2\text{B}_2\text{C}$, has the potential to clarify the effect of magnetic impurities on the superconducting state in the rare earth-nickel borocarbides.

II. EXPERIMENT

All samples in this study, $\text{Lu}_{1-x}\text{Gd}_x\text{Ni}_2\text{B}_2\text{C}$ and $\text{Y}_{1-x}\text{Gd}_x\text{Ni}_2\text{B}_2\text{C}$ series, were single crystals, grown using the Ni_2B high temperature growth technique^{7,28,29}. *As grown* crystals were used for this work. Gd concentrations in both series were evaluated through Curie-Weiss fits of the high-temperature part of magnetic susceptibility, that was measured using a Quantum Design, Magnetic Property Measurement System (MPMS) SQUID magnetometer. For resistance measurements a standard, four probe, ac technique ($f = 16$ Hz, $I = 0.2 - 2$ mA) with the current flowing in the ab plane, close to $I \parallel a$, was used. For these measurements platinum wires were attached to the samples using EpoTek H20E silver epoxy and the measurements were performed in a Quantum Design, Physical Property Measurement System (PPMS-14) instrument with ACT and He-3 options. $H_{c2}(T)$ data were obtained from temperature- and magnetic field-dependent resistance measurements. For these measurements $H \parallel c$ direction of the applied field was kept for all samples. Heat capacity measurements were performed in PPMS-14 instrument with He-3 option utilizing the relaxation technique with fitting of the whole temperature response of the microcalorimeter.

III. RESULTS AND DISCUSSION

A. Heat Capacity and $x - T$ Phase Diagram

Since the high temperature paramagnetism in the $\text{Lu}_{1-x}\text{Gd}_x\text{Ni}_2\text{B}_2\text{C}$ and $\text{Y}_{1-x}\text{Gd}_x\text{Ni}_2\text{B}_2\text{C}$ series is associated only with a local moment bearing Gd^{3+} ion, it was expedient to evaluate the real Gd concentration, x_{CW} , by fitting the measured dc susceptibility $\chi_{dc} = M/H$ (between ~ 150 K and room temperature) with $\chi_{dc} = x_{CW}C/(T - \Theta)$, where Θ is the Curie-Weiss temperature, $C = (N_A p_{eff}^2)/3k_B$, N_A is the Avogadro number, k_B is the Boltzmann constant, and p_{eff} is the effective moment (for Gd^{3+} $p_{eff} \approx 7.94\mu_B$). Fig 1 shows experimentally evaluated Gd concentration, x_{CW} as a function of the nominal concentration, $x_{nominal}$. For $\text{Y}_{1-x}\text{Gd}_x\text{Ni}_2\text{B}_2\text{C}$ both concentrations are very close to each other ($x_{CW}/x_{nominal} = 1.01(1)$), whereas the difference is fairly large in the case of

$\text{Lu}_{1-x}\text{Gd}_x\text{Ni}_2\text{B}_2\text{C}$ ($x_{CW}/x_{nominal} = 1.31(2)$); in both cases the dependence is close to linear in the range of concentrations studied. In the rest of the text, the experimentally determined Gd concentration will be used.

Normalized, zero-field, temperature-dependent resistivity data, $\rho(T)/\rho_{300K}$, for the $\text{Lu}_{1-x}\text{Gd}_x\text{Ni}_2\text{B}_2\text{C}$ and $\text{Y}_{1-x}\text{Gd}_x\text{Ni}_2\text{B}_2\text{C}$ series are shown in Fig. 2a and 2b. With Gd doping the residual resistivity ratio, $\text{RRR} = \rho_{300K}/\rho_n$, where ρ_n is the normal state resistivity just above the superconducting transition, decreases and the superconducting transition temperature, T_c , decreases as well (Fig. 2c, inset). The superconducting critical temperature determined from the onset of the resistive superconducting transition for $\text{Lu}_{1-x}\text{Gd}_x\text{Ni}_2\text{B}_2\text{C}$ and $\text{Y}_{1-x}\text{Gd}_x\text{Ni}_2\text{B}_2\text{C}$ is plotted as a function of Gd concentration in Fig. 2c. The $T_c(x)$ dependence is close to linear with a downturn seen in the case of $\text{Y}_{1-x}\text{Gd}_x\text{Ni}_2\text{B}_2\text{C}$ for the highest presented doping level. This behavior is consistent with Abrikosov-Gor'kov (AG) theory of pairbreaking on magnetic impurities². The rate of T_c suppression is similar for two $\text{R}_{1-x}\text{Gd}_x\text{Ni}_2\text{B}_2\text{C}$ series, being slightly higher for $\text{R} = \text{Lu}$. This difference is probably due to the additional contribution of the effect of non-magnetic scattering in superconductors with anisotropic gap. citemar63a,hoh63a,ope97a,kog10a Indeed, RRR (that can be, by Matthiessen's rule, roughly taken as a caliper of scattering, with lower RRR corresponding to higher scattering) decreases with Gd doping faster in the case of $\text{R} = \text{Lu}$ (Fig. 2c, inset), that is consistent with larger lattice mismatch (causing stronger scattering) for the Gd/Lu (in comparison to Gd/Y) substitution. For comparison, the data for $T_c(x)$ evolution in $\text{Lu}(\text{Ni}_{1-x}\text{Co}_x)_2\text{B}_2\text{C}$ from Ref. 34 are included in the same plot. It is noteworthy that the T_c suppression rate is higher for Co-doping to the Ni-site than for Gd-doping to the Lu(Y) site, even though among local moment rare earth (e.g. excluding Ce and Yb) Gd^{3+} (and Eu^{2+}) has the highest de Gennes factor, $(g_J - 1)^2 J(J + 1)$, and the strongest T_c suppression rate.^{7,10} The reason for such a strong effect of Co-substitution on T_c is at least two-fold: firstly, Co-substitution for Ni is not isoelectronic, it induces changes in the density of states at the Fermi level, therefore causing changes in T_c [35–37]; secondly, for similar concentrations, x , scattering appears to be stronger for Co-substitution (Fig.2c, inset), thus adding to the T_c suppressing rate.

Zero field, temperature-dependent heat capacity, $C_p(T)$, was measured for the $\text{Lu}_{1-x}\text{Gd}_x\text{Ni}_2\text{B}_2\text{C}$ and $\text{Y}_{1-x}\text{Gd}_x\text{Ni}_2\text{B}_2\text{C}$ series in order to get additional insight into the evolution of the magnetic properties with Gd-doping. The results are presented in Fig. 3. For

the parent compounds, and several lower Gd concentrations in each series, a jump in $C_p(T)$, at the superconducting transition temperature is clearly seen. This jump broadens with Gd-doping thus the value of ΔC_p at T_c was evaluated by the isentropic construct. Fig. 4 shows the heat capacity jump inferred from the isentropic construct for the $\text{Lu}_{1-x}\text{Gd}_x\text{Ni}_2\text{B}_2\text{C}$ and $\text{Y}_{1-x}\text{Gd}_x\text{Ni}_2\text{B}_2\text{C}$ series normalized to the value of the jump for the parent compounds, $\text{LuNi}_2\text{B}_2\text{C}$ and $\text{YNi}_2\text{B}_2\text{C}$, respectively, plotted as a function of normalized superconducting transition temperature, T_c/T_{c0} . As expected, the experimental points lay below the BCS law of corresponding states line,^{38,39} however these points also appear to be below the line obtained within the AG theory of pairbreaking from magnetic impurities⁴⁰ as well. Similar behavior of $\Delta C_p/\Delta C_{p0}$ vs T_c/T_{c0} was observed decades ago for Kondo-impurities (with temperature-dependent pair-breaking) in superconductors.^{41,42} In our case the dopant, Gd^{3+} , is a good local magnetic moment ion for which hybridization and Kondo-related physics are not expected. There are several possible explanations of such behavior that do not invoke the Kondo effect. Qualitatively similar behavior (approximated by $\Delta C_p \propto T^2$) was observed in $\text{Y}_{1-x}\text{R}_x\text{Ni}_2\text{B}_2\text{C}$ ($\text{R} = \text{Gd}, \text{Dy}, \text{Ho}, \text{and Er}$)⁴³ and was attributed to a combination of weak-coupling results of magnetic pairbreaking AG theory with strong coupling corrections. Alternatively, a Hartree-Fock approach by Shiba⁴⁴ yields a band of possible $\Delta C_p/\Delta C_{p0}$ vs T_c/T_{c0} values that is defined within this approach by the value of the parameter γ , related to the strength of spin-flip scattering. For $\gamma \rightarrow 1$ (weak scattering) the AG results reproduced. The limit of $\gamma \rightarrow 0$ describes strong spin-dependent scattering. Our experimental data lay close to this $\gamma \rightarrow 0$ limit (Fig. 4). Another possible explanation may be a combined effect of magnetic and nonmagnetic scattering⁴⁵ with a notion that the gap parameter in borocarbides is anisotropic. This last possibility is appealing but requires more theoretical work due to complexity of the theoretical results and a number of independent parameters required for a realistic description.

Our previous data on the $\text{Yb}_{1-x}\text{Gd}_x\text{Ni}_2\text{B}_2\text{C}$ and $\text{Lu}_{1-x}\text{Gd}_x\text{Ni}_2\text{B}_2\text{C}$ series¹⁸ provide experimental evidence that for Gd concentration $x \lesssim 0.3$ the long range magnetic order observed in pure $\text{GdNi}_2\text{B}_2\text{C}$ and the high-Gd end of the series, evolves into a spin glass (SG). A broad maximum in heat capacity marked as T_{max} in Fig. 3 is associated with a spin glass transition, with $T_{max} \approx 1.5T_f$, for RKKY spin glasses⁴⁶ where T_f is the spin glass freezing temperature.

The other feature in temperature-dependent heat capacity data (Fig. 3) is a broad min-

imum. This minimum exists for all of our $x > 0$ data and is most probably just a crossover between the low temperature magnetism-dominated behavior and high temperature behavior dominated by electron and phonon contributions.

Resistivity and heat capacity data together allow us to construct the $x-T$ phase diagram for the $\text{Lu}_{1-x}\text{Gd}_x\text{Ni}_2\text{B}_2\text{C}$ and $\text{Y}_{1-x}\text{Gd}_x\text{Ni}_2\text{B}_2\text{C}$ series (Fig. 5). As mentioned above, there is a slight difference in T_c variation with x between $R = \text{Lu}$ and $R = \text{Y}$. The other salient temperature, T_{max} , has very similar x -dependence in both cases. It has to be mentioned that probing magnetic signatures at temperatures below superconducting transition often is not a simple task. In electric/thermoelectric and low field magnetic susceptibility measurements the superconducting signal dominates. Magnetic field needed to suppress superconductivity might be large enough to alter fragile, low temperature, magnetic state (as it happens e.g. in materials with field-induced quantum critical point⁴⁷), or at a minimum, shift the phase line. Zero-field heat capacity measurements clearly reveal (complex) long range magnetic order below T_c .^{17,48} In the case of spin-glass transition heat capacity does not have clear anomaly at the freezing temperature, T_f , instead a broad maximum is detected at $\approx 1.5T_f$.⁴⁶ Having this in mind, we can approximately outline (by the dotted-dashed line in Fig. 5) the boundary of the spin-glass phase. Since, at least in zero-field resistivity, that was measured in this work down to the temperatures below the SG line for several Gd-concentrations, no reentrance behavior is observed, superconductivity coexists with the SG state at low temperatures. For slightly higher Gd concentrations, after superconductivity is just suppressed, (as it was mentioned for $\text{Lu}_{1-x}\text{Gd}_x\text{Ni}_2\text{B}_2\text{C}$ ¹⁸) spin-glass related behavior is observed both in heat capacity and magnetic susceptibility. On further Gd-doping, a long range magnetic order is established.

B. Upper Critical Field

The upper critical field was measured resistively, combining magnetic field-dependent data taken at constant temperature and temperature-dependent data taken in fixed magnetic field. Examples of such data for $\text{Lu}_{0.81}\text{Gd}_{0.19}\text{Ni}_2\text{B}_2\text{C}$ ($H\parallel c$) are shown in Figs. 6 (a) and (b). Re-entrant $R(T)$ curves for a few, relatively high, values of magnetic field (Fig. 6(b)) are noteworthy. Results obtained from both data sets are consistent, the resulting $H_{c2}(T)$ curves for two different criteria are shown in Fig. 6(c). The aforementioned re-entrant $R(T)$

curves are the results of the horizontal ($H = \text{constant}$) cuts through the shallow maximum in the $H_{c2}(T)$.

The $H_{c2}(T)$ data for the $\text{Lu}_{1-x}\text{Gd}_x\text{Ni}_2\text{B}_2\text{C}$ and $\text{Y}_{1-x}\text{Gd}_x\text{Ni}_2\text{B}_2\text{C}$ series are presented in Fig. 7. The evolution of the upper critical field behavior with Gd-doping is similar for both series: the behavior changes from monotonic with temperature for the parent and lightly-doped compounds to the behavior with shallow maximum for higher Gd concentrations. This evolution is seen better yet when plotted in normalized coordinates (Fig. 8). Qualitatively similar evolution of $H_{c2}(T)$ was theoretically described (in dirty limit) by taking into account paramagnetic effect.^{49,50} The use of dirty limit for this materials is consistent with previous studies.³⁴ The quantitative description of $H_{c2}(T)$ within a paramagnetic effect approach requires detailed knowledge of the paramagnetic contribution to susceptibility below T_c , which is a tedious task. On careful examination of Fig. 8(b) we can see that a noticeable broad maximum in $H_{c2}(T)$ is observed for $x = 0.14$ and $x = 0.21$, however this maximum practically disappears for the next concentration, $x = 0.26$, for which $H_{c2}(T)$ is monotonic with a tendency to saturation below $T/T_c \approx 0.5$. For this concentration (at zero field) the T_c value is close to T_f , the SG freezing temperature (Fig. 5). For spin glasses the paramagnetic component of susceptibility decreases below T_f [46] so that H_{c2} suppression is expected to be weaker, in agreement with our observation. Similar arguments were used in Ref. 51 for interpretation of $H_{c2}(T)$ data below the Néel temperature.

Fig. 9 presents the slope of the $H_{c2}(T)$ in the limit of $H \rightarrow 0$ as a function of T_c in zero field for the $\text{Lu}_{1-x}\text{Gd}_x\text{Ni}_2\text{B}_2\text{C}$ and $\text{Y}_{1-x}\text{Gd}_x\text{Ni}_2\text{B}_2\text{C}$ series. The observed behavior can be roughly approximated as $dH_{c2}/dT \propto T_c$. It is noteworthy that for several recently studied superconductors the behavior is qualitatively different: for $\text{Ce}_{1-x}\text{La}_x\text{CoIn}_5$ dH_{c2}/dT is approximately constant for $H\parallel c$ and has a factor of two larger absolute value with a slight positive slope for $H\parallel a$;⁵² for neutron-irradiated MgB_2 dH_{c2}/dT is approximately independent of T_c ,⁵³ whereas for carbon-doped MgB_2 $|dH_{c2}/dT|$ rapidly increases with decrease of T_c [54] (opposite to what is observed here); for Co-doped $\text{LuNi}_2\text{B}_2\text{C}$ the derivative decreases in the absolute value only by $\approx 20\%$ when T_c decreases approximately by half.³⁴

It is worth mentioning that $dH_{c2}/dT \propto T_c$ is predicted for isotropic s -wave materials in the clean limit. As discussed above, such description appear not to be pertinent to the borocarbides. On the other hand, such proportionality is a property of the AG gapless state^{2,33,55} and is present (at least approximately) in the data from elemental La doped

with Gd [56] (the data in the publication need to be reanalyzed to extract the derivatives). Recently, similar behavior was observed in 1111 family of Fe-As superconductors and was attributed to pair-breaking in anisotropic superconductors.⁵⁵

Following Ref. 55, $|d(dH_{c2}/dT)/dT_c| \propto \pi\phi_0 k_B^2/\hbar^2 v^2$, where ϕ_0 is the flux quantum, k_B is the Boltzmann constant and v is the Fermi velocity. Since $|d(dH_{c2}/dT)/dT_c| \approx 0.25$ kOe/K² (Fig. 9), the order of magnitude estimate gives $v \sim 3 \times 10^7$ cm/s. This estimate is consistent with the values used to describe superconductivity in parent LuNi₂B₂C and YNi₂B₂C.^{57,58}

IV. SUMMARY

Gd-doping of LuNi₂B₂C and YNi₂B₂C results in T_c suppression, consistent with AG magnetic pairbreaking with possible additional contribution from non-magnetic scattering in materials with anisotropic gaps. For both series T_c is suppressed to zero by 30-35% Gd substitution. The $x - T$ phase diagram reveals a region of co-existence between superconductivity and a spin-glass state arising from the Gd-magnetism. The evolution of the temperature-dependent H_{c2} with Gd-doping can be understood by taking into account the paramagnetic effect and, for the superconducting sample with highest Gd-concentration in this study, Y_{0.74}Gd_{0.26}Ni₂B₂C, by considering temperature dependence of paramagnetic susceptibility below the SG freezing temperature. The H_{c2} derivatives in the limit of $H \rightarrow 0$ are approximately linear with zero-field superconducting transition temperatures, in agreement with the behavior expected for AG pairbreaking.

All in all, the Lu_{1-x}Gd_xNi₂B₂C and Y_{1-x}Gd_xNi₂B₂C series present viable systems for studies of magnetic pairbreaking in anisotropic superconductors and interplay of superconductivity and spin glass state.

Acknowledgments

Work at the Ames Laboratory was supported by the US Department of Energy - Basic Energy Sciences under Contract No. DE-AC02-07CH11358. This manuscript was finalized

during the Ames floods of 2010, the second "hundred year floods" in a 15 year time span.

- ¹ P. W. Anderson, Phys. Rev. Lett. **3**, 325 (1959).
- ² A. A. Abrikosov and L. P. Gor'kov, Zh. Exper. Teor. Fiz. **39**, 1781 (1960) [Sov. Phys. JETP **12**, 1243 (1961)].
- ³ A. V. Balatsky, I. Vekhter, and J.-X. Zhu, Rev. Mod. Phys **78**, 373 (2006).
- ⁴ R. Ramazashvili and P. Coleman, Phys. Rev. Lett. **79**, 3752 (1997).
- ⁵ V. P. Mineev and M. Sigrist, Phys. Rev. B **63**, 172504 (2001).
- ⁶ N. Shah and A. Lopatin, Phys. Rev. B **76**, 094511 (2007).
- ⁷ P. C. Canfield, P. L. Gammel, and D. J. Bishop, Physics Today **51**(10), 40 (1998).
- ⁸ K. H. Müller and V. N. Narozhnyi, Rep. Progr. Phys. **64**, 943 (2001).
- ⁹ K. H. Müller, G. Fuchs, S. L. Drechsler, and V. N. Narozhnyi, in *Handbook of Magnetic Materials*, edited by K. H. J. Buschow (North-Holland, Amsterdam, 2002) vol. 14, p. 199.
- ¹⁰ S. L. Bud'ko and P. C. Canfield, C. R. Physique **7**, 56 (2006).
- ¹¹ G. Wang and K. Maki, Phys. Rev. B **58**, 6493 (1998).
- ¹² K. Maki, P. Thalmeier, and H. Won, Phys. Rev. B **65**, 140502 (2002).
- ¹³ Q. Yuan and P. Thalmeier, Phys. Rev. B **68**, 174501 (2003).
- ¹⁴ Q. Yuan, H.-Y. Chen, H. Won, S. Lee, K. Maki, P. Thalmeier, and C. S. Ting, Phys. Rev. B **68**, 174510 (2003).
- ¹⁵ K. Maki, H. Won, and S. Haas, Phys. Rev. B **69**, 012502 (2004).
- ¹⁶ R. Movshovich, M. F. Hundley, J. D. Thompson, P. C. Canfield, B. K. Cho, and A. V. Chubukov, Physica C **227**, 381 (1994).
- ¹⁷ R. A. Ribeiro, S. L. Bud'ko, and P. C. Canfield, J. Magn. Magn. Mat. **267**, 216 (2003).
- ¹⁸ S. L. Bud'ko, J. D. Strand, N. E. Anderson, R. A. Ribeiro, and P. C. Canfield, Phys. Rev. B **68**, 104417 (2003).
- ¹⁹ M. E. Massalami, S. L. Bud'ko, B. Giordanengo, M. B. Fontes, J. C. Mondragon, and E. M. Baggio-Saitovitch, Physica C **235-240**, 2563 (1994).
- ²⁰ M. E. Massalami, S. L. Bud'ko, B. Giordanengo, M. B. Fontes, J. C. Mondragon, E. M. Baggio-Saitovitch, and A. Sulpice, Phys. Stat. Sol. B **189**, 489 (1995).
- ²¹ P. G. Pagliuso, C. Rettori, S. B. Oseroff, P. C. Canfield, and E. M. Baggio-Saitovitch, Phys.

- Rev. B **57**, 3668 (1998).
- ²² M. D. Lan, T. J. Chang, and C. S. Liaw, J. Phys. Chem. Solids **59**, 1285 (1998).
 - ²³ M. El-Hagary, H. Michor, and G. Hilscher, Phys. Rev. B **61**, 11695 (2000).
 - ²⁴ H. Michor, M. El-Hagary, L. Haber, E. Bauer, and G. Hilscher, Phys. Rev. B **61**, 6487 (2000).
 - ²⁵ Z. Drzazga, G. Fuchs, A. Handstein, K. Nenkov, and K. H. Müller, Physica C **383**, 421 (2003).
 - ²⁶ B. K. Cho, P. C. Canfield, and D. C. Johnston, Phys. Rev. Lett. **77**, 163 (1996).
 - ²⁷ K. D. D. Rathnayaka, D. G. Naugle, A. C. Dumar, M. P. Anatska, and P. C. Canfield, Int. J. Mod. Phys. B **17**, 3493 (2003).
 - ²⁸ Ming Xu, P. C. Canfield, J. E. Ostenson, D. K. Finnemore, B. K. Cho, Z. R. Wang, and D. C. Johnston, Physica C **227**, 321 (1994).
 - ²⁹ P. C. Canfield, and I. R. Fisher, J. Crystal Growth **225**, 155 (2001).
 - ³⁰ D. Markowitz, and L. P. Kadanoff, Phys. Rev. **131**, 563 (1963).
 - ³¹ P. Hohenberg, Zh. Eksp. Teor. Fiz. **45**, 1208 (1963) [Sov. Phys. JETP **18**, 834 (1964)].
 - ³² L. A. Openov, Pis'ma Zh. Eksp. Teor. Fiz. **66**, 627 (1997) [JETP Lett. **66**, 661 (1997)].
 - ³³ V. G. Kogan, Phys. Rev. B **81**, 184528 (2010).
 - ³⁴ K. O. Cheon, I. R. Fisher, V. G. Kogan, P. C. Canfield, P. Miranović, and P. L. Gammel, Phys. Rev. B **58**, 6463 (1998).
 - ³⁵ H. Schmidt, M. Mueller, and H. F. Braun, Physica C **235-240**, 779 (1994).
 - ³⁶ S. L. Bud'ko, M. Elmassalami, M. B. Fontes, J. Mondragon, W. Vanoni, B. Giordanengo, and E. M. Baggio-Saitovitch, Physica C **243**, 183 (1995).
 - ³⁷ L. F. Mattheiss, Phys. Rev. B **49**, 13279 (1994).
 - ³⁸ J. Bardeen, L. N. Cooper, and J. R. Schrieffer, Phys. Rev. **108**, 1175 (1957).
 - ³⁹ James C. Swihart, Phys. Rev. **116**, 346 (1959).
 - ⁴⁰ S. Skalski, O. Betbeder-Matibet, and P. R. Weiss, Phys. Rev. **136**, A1500 (1964).
 - ⁴¹ E. Müller-Hartmann, and J. Zittartz, Solid State Comm. **11**, 401 (1972).
 - ⁴² M. Brian Maple, Appl. Phys. **9**, 179 (1976).
 - ⁴³ M. El-Hagary, H. Michor, and G. Hilscher, Phys. Rev. B **61**, 11695 (2000).
 - ⁴⁴ Hiroyuki Shiba, Prog. Theor. Phys. **50** 50 (1973).
 - ⁴⁵ Leonid A. Openov, Phys. Rev. B **69** 224516 (2004).
 - ⁴⁶ J. A. Mydosh, *Spin Glasses: An Experimental Introduction* (Taylor & Francis, London, 1993).
 - ⁴⁷ G. R. Stewart, Rev. Mod. Phys. **73**, 797 (2001); *ibid.* **78**, 743 (2006).

- ⁴⁸ B. K. Cho, P. C. Canfield, L. L. Miller, D. C. Johnston, W. P. Beyermann, and A. Yatskar, Phys. Rev. B **52**, 3684 (1995).
- ⁴⁹ K. Maki, Physics **1**, 127 (1964).
- ⁵⁰ D. Saint-James, G. Sarma, and E. J. Thomas *Type II Superconductivity* (Pergamon Press, Oxford, 1969).
- ⁵¹ A. I. Buzdin and L. N. Bulaevskii, Usp. Fiz. Nauk **149**, 45 (1986) [Sov. Phys. Uspekhi **29**, 412 (1986)].
- ⁵² C. Petrovic, S. L. Bud'ko, V. G. Kogan, and P. C. Canfield, Phys. Rev. B **66**, 054534 (2002).
- ⁵³ R. H. T. Wilke, S. L. Bud'ko, P. C. Canfield, J. Farmer, and S. T. Hannahs, Phys. Rev. B **73**, 134512 (2006).
- ⁵⁴ R. H. T. Wilke, S. L. Bud'ko, P. C. Canfield, D. K. Finnemore, Raymond J. Suplinskas, and S. T. Hannahs, Phys. Rev. Lett. **92**, 217003 (2004).
- ⁵⁵ V. G. Kogan, Phys. Rev. B **80**, 214532 (2009).
- ⁵⁶ P. M. Chaikin and T. W. Mihalishin, Phys. Rev. B **6**, 839 (1972).
- ⁵⁷ V. G. Kogan, M. Bullock, B. Harmon, P. Miranović, Lj. Dobrosavljević-Grujić, P. L. Gammel, and D. J. Bishop, Phys. Rev. B **55**, 8693 (1997).
- ⁵⁸ S. V. Shulga, S.-L. Drechsler, G. Fuchs, K.-H. Müller, K. Winzer, M. Heinecke, and K. Krug, Phys. Rev. Lett. **80**, 1730 (1998).

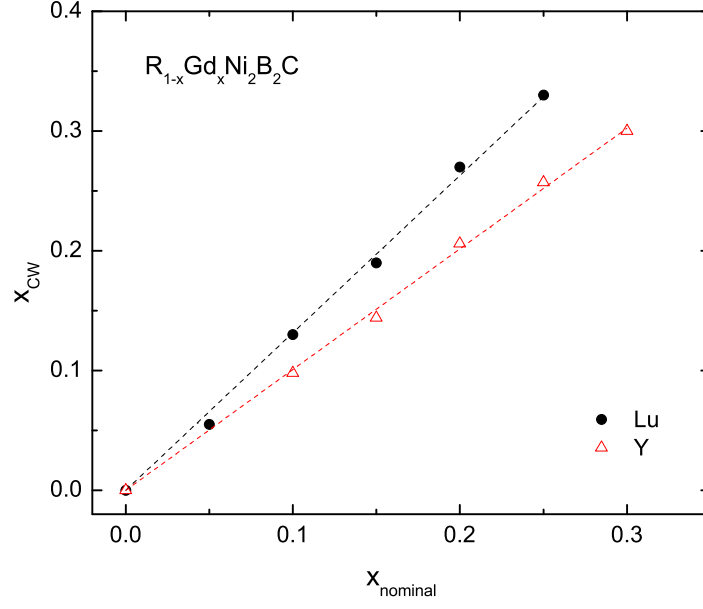


FIG. 1: (Color online) Gd-concentration evaluated from a Curie-Weiss fit of the high temperature susceptibility vs nominal Gd-concentration in $R_{1-x}\text{Gd}_x\text{Ni}_2\text{B}_2\text{C}$, $R = \text{Lu}, \text{Y}$. Dashed lines are linear fits with intercept fixed to zero. (see text for details)

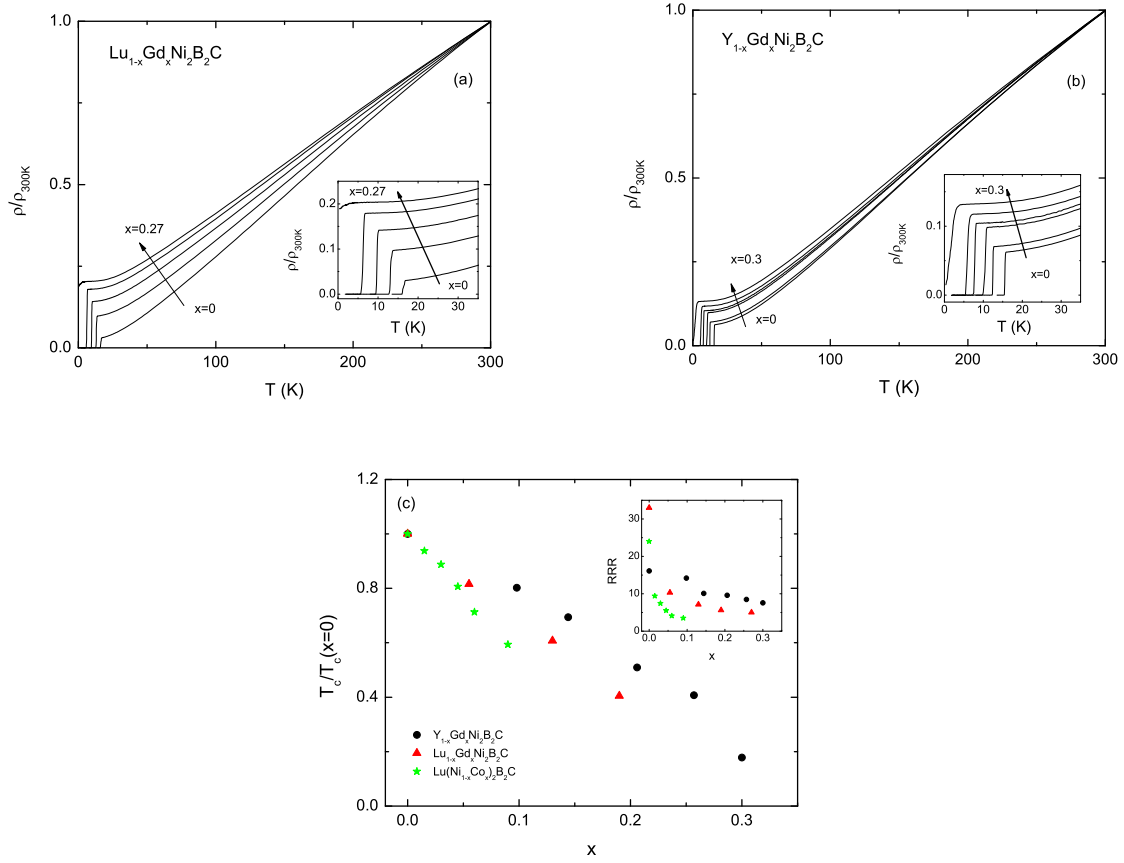


FIG. 2: (Color online) Normalized resistivity, ρ/ρ_{300K} for (a) $\text{Lu}_{1-x}\text{Gd}_x\text{Ni}_2\text{B}_2\text{C}$ ($x = 0, 0.055, 0.13, 0.19, 0.27$), and (b) $\text{Y}_{1-x}\text{Gd}_x\text{Ni}_2\text{B}_2\text{C}$ ($x = 0, 0.10, 0.14, 0.21, 0.26, 0.30$). Arrows show the direction of increasing x , insets: low temperature part of the data. Panel (c): Normalized (to the values for the parent compounds) T_c as a function of Gd concentration x for $\text{R}_{1-x}\text{Gd}_x\text{Ni}_2\text{B}_2\text{C}$, $\text{R} = \text{Lu}, \text{Y}$; data for $\text{Lu}(\text{Ni}_{1-x}\text{Co}_x)_2\text{B}_2\text{C}$ from Ref. 34 are included for comparison. Inset: RRR vs x for the same three series.

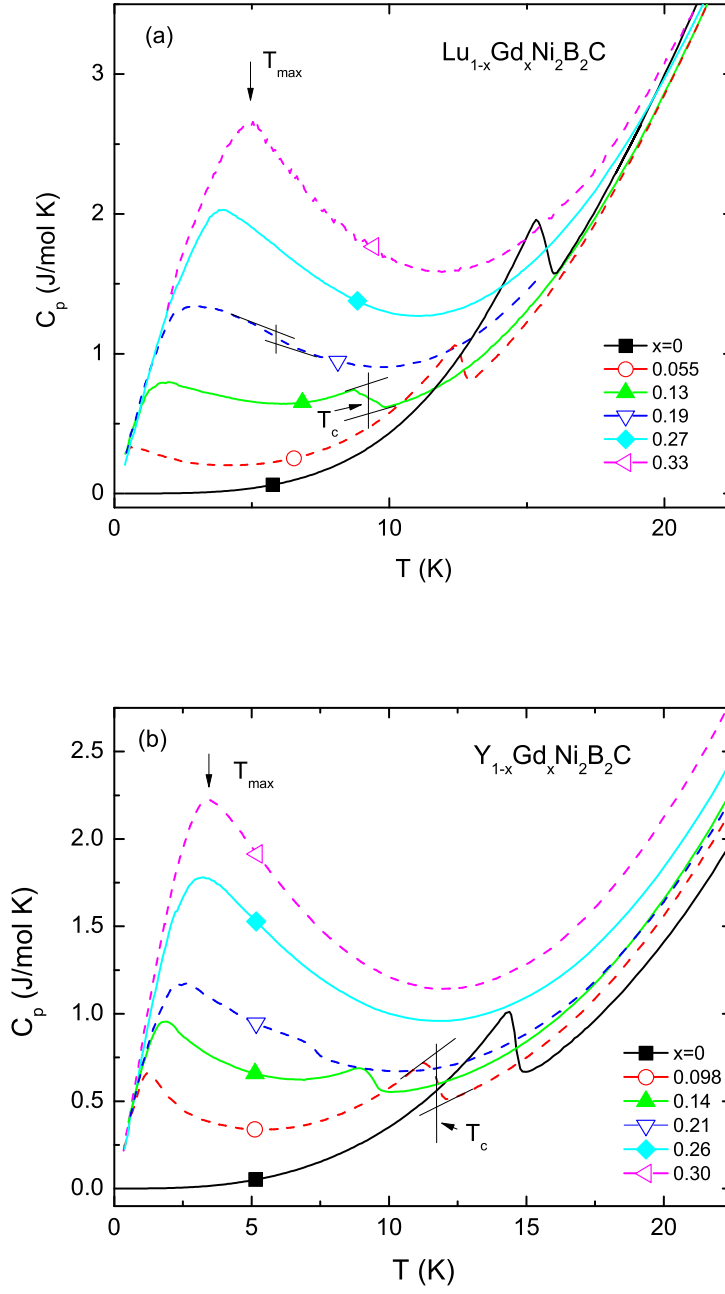


FIG. 3: (Color online) Temperature dependent heat capacity for (a) $\text{Lu}_{1-x}\text{Gd}_x\text{Ni}_2\text{B}_2\text{C}$ ($x = 0, 0.055, 0.13, 0.19, 0.27, 0.33$), and (b) $\text{Y}_{1-x}\text{Gd}_x\text{Ni}_2\text{B}_2\text{C}$ ($x = 0, 0.10, 0.14, 0.21, 0.26, 0.30$). Arrows show examples of how T_{\max} and T_c are determined.

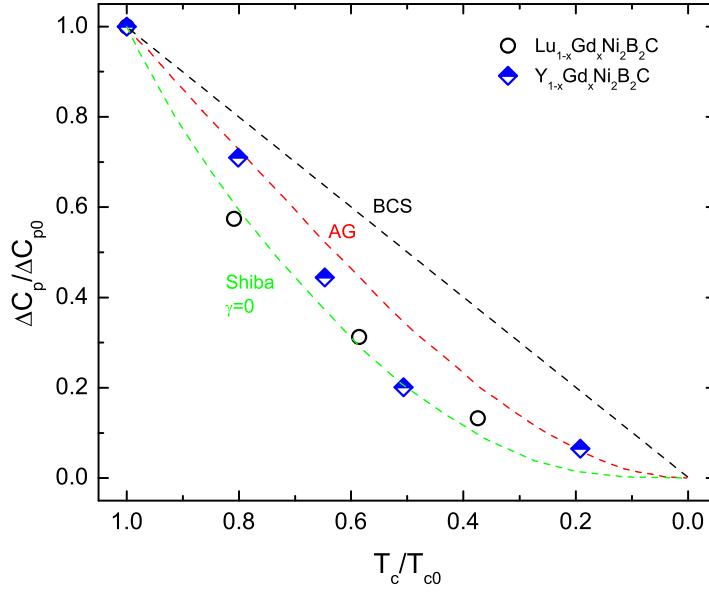


FIG. 4: (Color online) Normalized jump in heat capacity at T_c vs normalized T_c for the $\text{Lu}_{1-x}\text{Gd}_x\text{Ni}_2\text{B}_2\text{C}$ and $\text{Y}_{1-x}\text{Gd}_x\text{Ni}_2\text{B}_2\text{C}$ series. Dashed lines correspond to BCS law of corresponding states, Abrikosov-Gor'kov magnetic scattering, and $\gamma = 0$ (strong spin-dependent scattering) limit of Shiba's theory.⁴⁴ See text for more details.

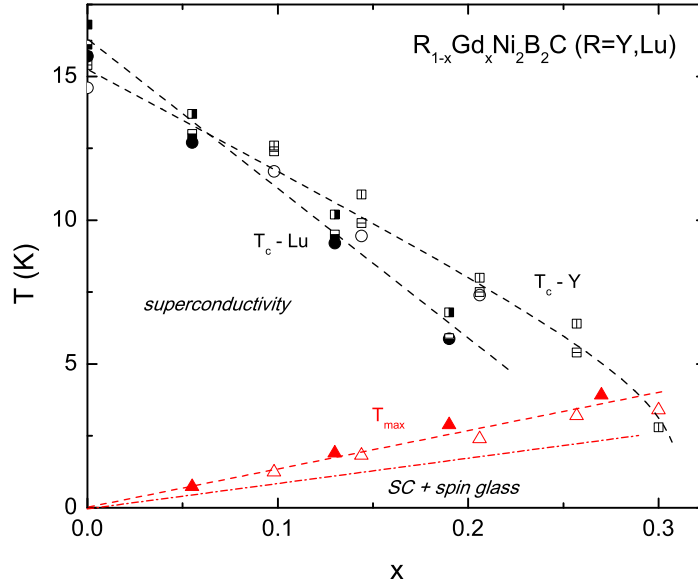


FIG. 5: (Color online) $T - x$ phase diagram for the $\text{Lu}_{1-x}\text{Gd}_x\text{Ni}_2\text{B}_2\text{C}$ (filled and partially filled symbols) and $\text{Y}_{1-x}\text{Gd}_x\text{Ni}_2\text{B}_2\text{C}$ (open symbols) series. Symbols: squares - T_c from onset and offset of the resistive transitions; circles - T_c from heat capacity; triangles - T_{max} from heat capacity. Dashed lines are guides for the eye. Dotted-dashed line approximates spin-glass phase (crossover) line.

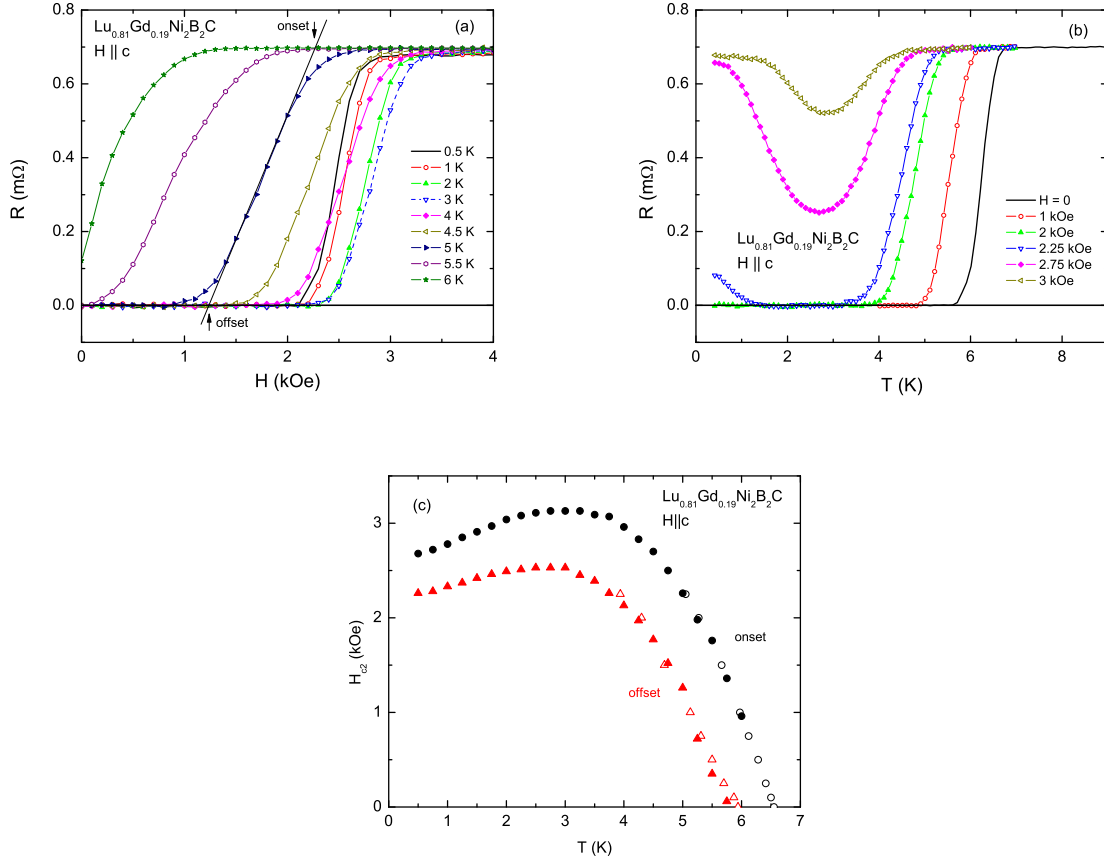


FIG. 6: (Color online) (a) Examples of magnetic field-dependent resistance of $\text{Lu}_{0.81}\text{Gd}_{0.19}\text{Ni}_2\text{B}_2\text{C}$ single crystal measured at several constant temperatures for $H \parallel c$. Onset and offset criteria of superconducting transition are illustrated. (b) Examples of temperature-dependent resistance of the same sample measured in different applied magnetic fields. (c) Temperature-dependent upper critical field of $\text{Lu}_{0.81}\text{Gd}_{0.19}\text{Ni}_2\text{B}_2\text{C}$ for $H \parallel c$. Circles - onset, triangles - offset, open symbols are from $R(T)|_H$ scans, filled symbols are from $R(H)|_T$ scans.

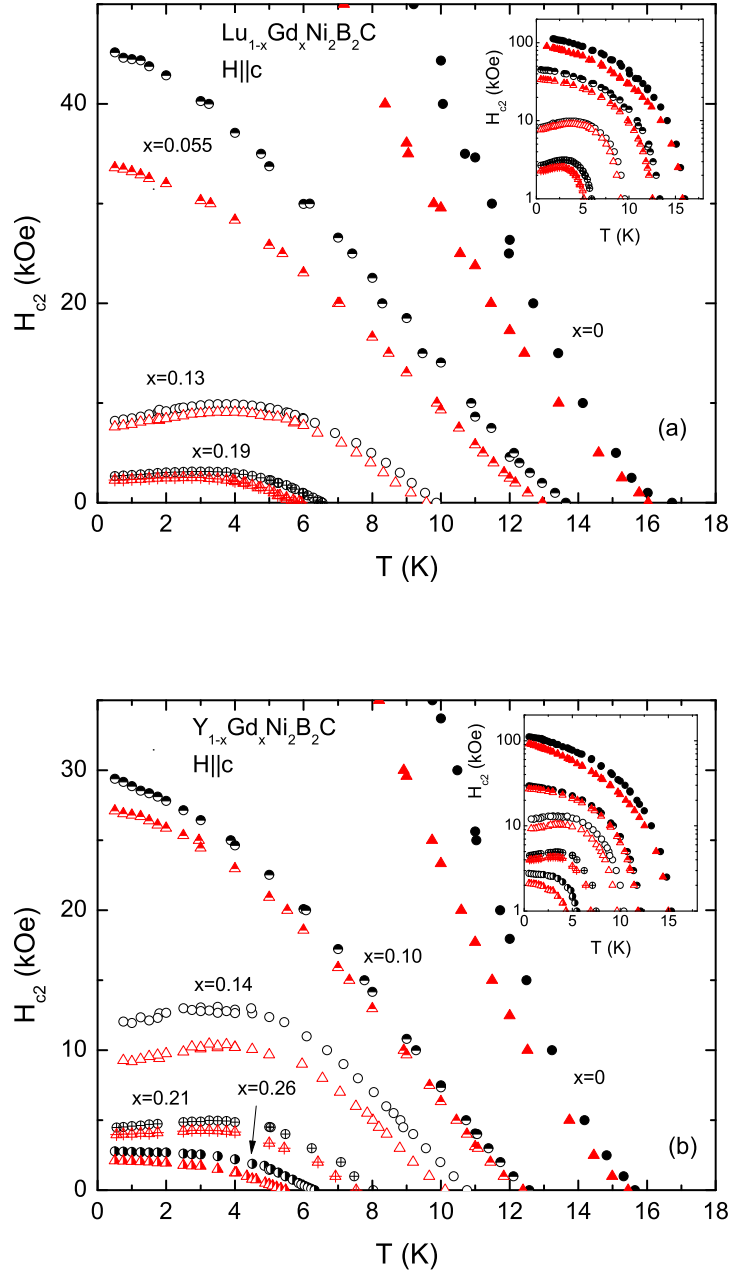


FIG. 7: (Color online) Temperature dependent upper critical field ($H \parallel c$) for (a) $\text{Lu}_{1-x}\text{Gd}_x\text{Ni}_2\text{B}_2\text{C}$ ($x = 0, 0.055, 0.13, 0.19$), and (b) $\text{Y}_{1-x}\text{Gd}_x\text{Ni}_2\text{B}_2\text{C}$ ($x = 0, 0.10, 0.14, 0.21, 0.26$). Circles and triangles correspond to the onset and offset criteria respectively. Insets show the same data on a semi-log scale.

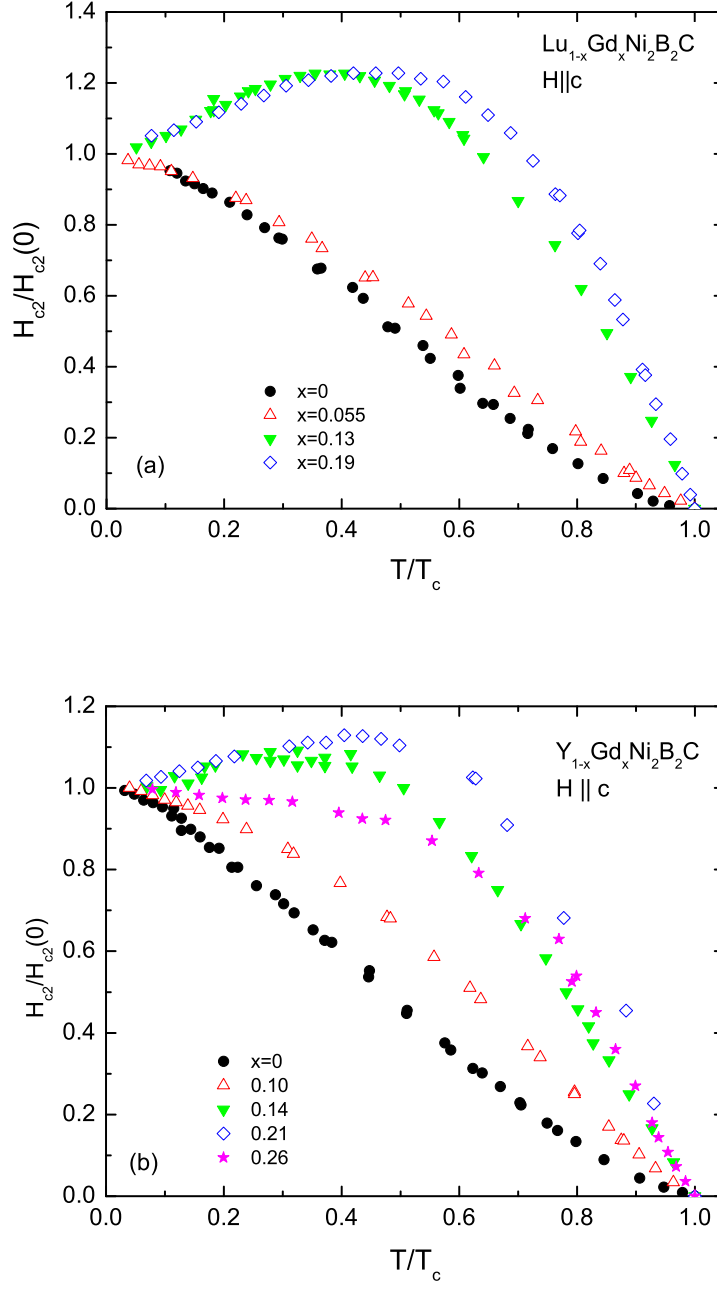


FIG. 8: (Color online) Normalized to $H_{c2}(T = 0)$ temperature dependent upper critical field for (a) $\text{Lu}_{1-x}\text{Gd}_x\text{Ni}_2\text{B}_2\text{C}$ ($x = 0, 0.055, 0.13, 0.19$), and (b) $\text{Y}_{1-x}\text{Gd}_x\text{Ni}_2\text{B}_2\text{C}$ ($x = 0, 0.10, 0.14, 0.21, 0.26$) as a function of normalized to $T_c(H = 0)$ temperature. Data for $H \parallel c$ obtained using onset criteria are shown.

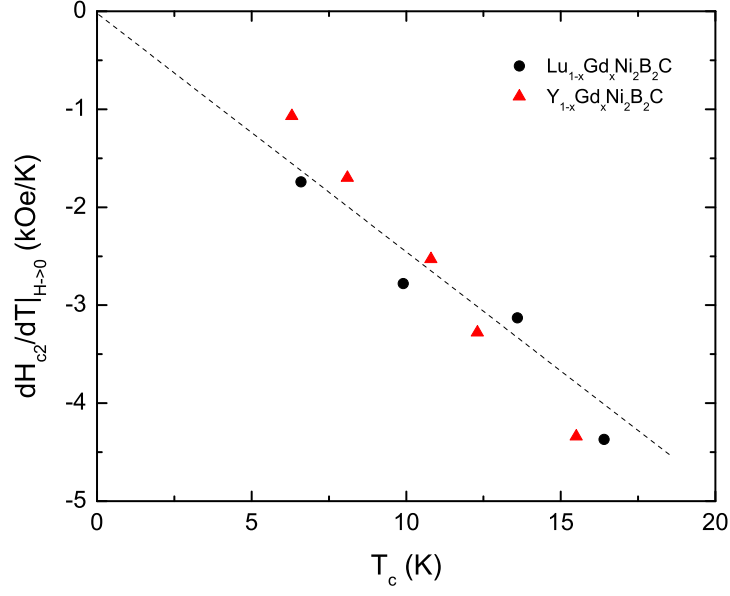


FIG. 9: (Color online) dH_{c2}/dT in the $H \rightarrow 0$ limit as a function of T_c in zero field for the $\text{Lu}_{1-x}\text{Gd}_x\text{Ni}_2\text{B}_2\text{C}$ (circles) and $\text{Y}_{1-x}\text{Gd}_x\text{Ni}_2\text{B}_2\text{C}$ (triangles) series. Dashed line is a guide to the eye.